JAMES | Journal of Advances in Modeling Earth Systems

RESEARCH ARTICLE
10.1029/2019MS001717

Effects of Topography and Realistic Drag on the Southern Hemisphere Midlatitude Jet in a Dry Model

F. Pithan[1] **and I. Polichtchouk**[2]

[1]Alfred Wegener Institut, Helmholtz Centre for Polar and Marine Research, Bremerhaven, Germany, [2]European Centre for Medium-Range Weather Forecasts, Reading, UK

Key Points:
- Using quadratic instead of linear drag can reverse the midlatitude jet response to drag changes
- Enhanced drag over land shifts the SH jet poleward in a model with topography and quadratic drag
- Intermodel differences in the dry dynamics setup have a strong impact on the jet latitude

Correspondence to:
F. Pithan,
felix.pithan@awi.de

Citation:
Pithan, F., & Polichtchouk, I. (2020). Effects of topography and realistic drag on the Southern Hemisphere midlatitude jet in a dry model. *Journal of Advances in Modeling Earth Systems*, *12*, e2019MS001717. https://doi.org/10.1029/2019MS001717

Received 15 APR 2019
Accepted 13 FEB 2020
Accepted article online 18 FEB 2020

Abstract Climate models have substantial biases in the climatological latitude of the Southern Hemisphere eddy-driven jet and the time scale of annular mode variability and disagree on the jet response to climate change. Zonally symmetric dry dynamical cores are often used for idealized modeling of the jet response to forcing and its sensitivity to model setup changes. The limits to which these models represent the key mechanisms that control the jet in complex models or the real world have not been systematically investigated. Here we show that substantial intermodel differences in jet latitude and strength can arise from differences in dynamical cores and resolved topography. Including topography and a more realistic surface drag in a dry model substantially alters the jet response to changes in drag strength. Using real-world maps, enhanced drag over land shifts the jet poleward, whereas enhanced drag over the ocean leads to an equatorward shift. No universal relationship between annular mode time scale and forced response emerges in the dry model with topography. These results suggest that zonally symmetric models with Rayleigh drag lack important mechanisms that control the behavior of the midlatitude jet in coupled climate models. A dry model with topography and quadratic surface drag can fill this gap in the model hierarchy.

Plain Language Summary Weather and climate models struggle to correctly represent the midlatitude westerlies and often place them too far equatorward in the Southern Hemisphere. Reduced models that omit the effects of moisture and clouds and have a very simple representation of surface drag are often used to study how the westerlies respond to different forcings. Here we show that the response of the midlatitude westerlies to forcings can change dramatically when a slightly more realistic representation of surface drag is used in a model. We also show that large differences between models can arise from the way a model is constructed, independently of the representation of physical processes such as surface friction.

1. Introduction

Understanding what controls the strength, latitude, and variability of the midlatitude eddy-driven jet is a fundamental research question with substantial implications for society. The configuration of the jet not only affects wind speeds but can also lead to temperature and precipitation extremes including cold spells, heat waves, and droughts (Cohen et al., 2014). Therefore, it would be highly beneficial to accurately represent eddy-driven jet configuration in numerical weather and climate prediction models and to confidently predict the midlatitude jet response to climate change. However, climate models show a large spread in the jet response to climate change and even struggle to reproduce the climatological jet characteristics in a present-day climate (Shepherd, 2014). Few aspects of the jet response to climate change are thoroughly understood theoretically, making it hard to disentangle the trustworthy aspects of the response in coupled models (Bony et al., 2015).

In particular, models often misplace the climatological jet latitude, with a tendency toward an equatorward bias in current climate models (Simpson & Polvani, 2016). The time scale of Southern Hemisphere jet variability in models is frequently too long, in particular in austral summer (Gerber et al., 2008). In the annual mean, these jet characteristics correlate with the jet response to climate change in Coupled Model Intercomparison Project Phase 5 (CMIP5) models (Kidston & Gerber, 2010). In particular, models with longer time scales of jet variability in the present-day climate have larger equatorward jet biases and tend to shift the jet further poleward in future climates, compared to models with shorter time scales of jet variability. It has

been suggested that long time scales of variability are a sign of weak negative feedbacks to departures from the mean state and that these weak negative feedbacks would also cause a stronger response to external forcing (Ring & Plumb, 2008). A robust relationship between biases in the present-day climate and projected climate change across a model ensemble can potentially be used to constrain the future response and thus obtain a more reliable estimate than given by the multimodel mean.

However, a physical mechanism that causes the above described correlations remains to be established. Recent work has shown that the annual-mean relationship between time scale of variability and jet shift does not hold in individual seasons and may just emerge by the conflation of signals from different seasons (Simpson & Polvani, 2016). We therefore require a better understanding of the physical mechanisms that control jet characteristics.

Simplified models of the Earth's atmosphere are important tools to build our understanding (Held, 2005). Such models retain the key mechanisms controlling the behavior or phenomenon of interest but omit details in order to simplify the analysis and understanding of results and allow for a larger number of numerical experiments to be performed. Many studies on the midlatitude jet, including its response to forcing (e.g., climate change, mechanical forcing, changes in surface drag, and presence or absence of the stratospheric polar vortex), and the relationship between the time scale of internal variability and the response to forcing, have been performed with the "Held-Suarez" setup (Held & Suarez, 1994). In this setup dry dynamical cores are driven by the relaxation of temperature to a zonally symmetric background state (Newtonian relaxation) and of the near-surface horizontal winds to 0 on a given time scale (Rayleigh drag).

While this simple setup has proven to be extremely useful in developing fundamental theoretical understanding of atmospheric circulation, it is not clear nor has it been systematically investigated if it actually contains the key mechanisms that control the latitude, speed, and variability of the midlatitude jet across climate model ensembles or in the real world. Too simple setups that omit important mechanisms could be the reason for disagreement of results at different levels of the model hierarchy.

For example, dry models without topography show an equatorward shift of the midlatitude jet with increased surface drag (Chen et al., 2007; Mbengue & Woollings, 2019). Robinson (1997) showed this to be caused by the Rayleigh drag acting on the mean flow rather than the eddies and argued that friction changes how the zonal wind responds to eddy forcing. Note that a convenient feature of the linear Rayleigh drag is that in spectral dynamical cores it is possible to independently vary the drag on different spherical harmonics to assess the effect of drag on different scales. This is no longer possible by using more realistic quadratic drag formulation. James and Gray (1986) described the barotropic governor effect, by which strong horizontal, barotropic shears made possible by low surface drag act to suppress baroclinicity, resulting in the seemingly paradox behavior of lower surface drag leading to weaker baroclinic activity. However, sensitivity experiments with complex climate models suggest that adding localized low-level drag over topography acts to shift the Southern Hemisphere jet poleward (Pithan et al., 2016; van Niekerk et al., 2017).

Aquaplanet experiments have shown that changing the surface turbulent fluxes over ocean mostly impacts the midlatitude jet through heat and moisture rather than momentum fluxes (Polichtchouk & Shepherd, 2016). The present paper therefore focuses on topographic drag, which has no first-order effect on the heat and moisture budgets. While Brayshaw et al. (2009) and Wilson et al. (2009) used a full-physics climate model with simplified continental configurations and an intermediate general circulation model coupled to an ocean to understand how mountains, land-sea contrasts and ocean dynamics shape the storm tracks, here we rely on a slightly modified dry dynamical core to keep the computations as simple and traceable as possible.

In particular, we add realistic topography and a more realistic surface drag—which quadratically depends on wind speed—to the Held-Suarez-type model. The effect of adding realistic topography on the Northern Hemisphere storm tracks in such models has been previously investigated by Chang (2009) under longitudinally varying thermal forcing. Here we focus on the Southern Hemisphere and use zonally symmetric thermal forcing to understand midlatitude jet behavior. We focus on (1) the role of dynamical cores and resolved topography versus that of diabatic processes for intermodel differences, (2) the effect of surface drag on the jet, and (3) the relationships between the time scale of jet variability, jet latitude, and the forced response.

2. Methods

2.1. Models

We use the Max Planck Institute's Icosahedral Nonhydrostatic model ICON version 2.0 with the r2b4 grid corresponding to a resolution of about 150 km (Giorgetta et al., 2018) and Community Atmosphere Model, version 5 (CAM5) with finite-volume hydrostatic dynamical core at 1.5° × 2.5° horizontal resolution (Neale et al., 2010). Model top is at 83 km, that is, a pressure lower than 1 Pa in ICON and 291.7 Pa in CAM5. The vertical resolution is 47 levels for ICON and 26 levels for CAM5, with the lowest full level at 20 (ICON) and 70 m (CAM5). Both models are used in Held-Suarez mode; that is, all physics schemes are switched off and replaced by Newtonian relaxation and Rayleigh drag. The setup follows Held and Suarez (1994) except for the addition of a hemispheric asymmetry in the background temperature as in McGraw and Barnes (2016) to obtain Southern Hemisphere winter and summer conditions. Zonally symmetric thermal forcing is prescribed in all our experiments. In contrast to Chang (2009), who relaxed temperature to a longitudinally varying background field, thermal land-sea contrasts or feedbacks of storm tracks on the diabatic heating are not considered in our experiments. In some experiments, we additionally add a temperature gradient in the stratosphere to obtain a stratospheric polar vortex as in Polvani and Kushner (2002). Zonally symmetric heating in the upper tropical troposphere is used as a simple climate change like forcing following McGraw and Barnes (2016).

In contrast to the original Held-Suarez setup, a realistic resolved topography is used in our experiments unless stated otherwise. The pressure drag exerted by topography thereby enters into the momentum equation to the extent that the topography is resolved by the model grid:

$$\frac{D\vec{u}}{Dt} = -2\vec{\Omega} \times \vec{u} - \frac{\nabla p}{\rho} - g\nabla h + F_{turb}, \tag{1}$$

that is, the Lagrangian (material) derivative of the horizontal wind vector $\frac{D\vec{u}}{Dt}$ is given by the Coriolis force $-2\vec{\Omega} \times \vec{u}$, the pressure gradient force $\frac{\nabla p}{\rho}$, the resolved pressure drag at the surface $-g\nabla h$, and the turbulent friction F_{turb}, where ∇p is the horizontal pressure gradient, ρ the density, p_{surf} surface pressure, g is gravitational acceleration, and ∇h the horizonal gradient of surface height. Note that the horizontal components of the Earth's rotation velocity $\vec{\Omega}$ are neglected in CAM.

In the standard Held-Suarez setup without topography, the resolved pressure drag is 0 and turbulent friction is represented by Rayleigh drag $F_{turb} = -\frac{\vec{u}}{\tau_F}$, where τ_F is the friction time scale. In some of our experiments (see Table 1), the linear Rayleigh drag is replaced with a drag that quadratically depends on near-surface wind. At the surface, this simple drag scheme takes the form $F_{turb} = -c_d|\vec{u}|\vec{u}$ (Reed & Jablonowski, 2012). The drag coefficient c_d is a surface-depended constant (see below). While Rayleigh drag directly extracts momentum at all levels it is applied to, the quadratic drag scheme only extracts momentum at the surface, that is, from the lowest model level. Away from the surface, F_{turb} becomes the divergence of the vertical momentum flux $F_{turb} = \frac{\partial F_z}{\partial z}$. The vertical momentum flux is computed as the product of the vertical gradient of horizontal winds and a prescribed eddy diffusivity, $F_z = -K_m \frac{d\vec{u}}{dz}$. The eddy diffusivity is as follows:

$$K_m = \begin{cases} c_d|\vec{u}_a|z_a, & \text{for} \quad \sigma \geq \sigma_{top} \\ c_d|\vec{u}_a|z_a exp\left(-\left[\frac{\sigma_{top}-\sigma}{\sigma_{strato}}\right]^2\right), & \text{for} \quad \sigma < \sigma_{top}, \end{cases} \tag{2}$$

where $\vec{u}_a$ and z_a are the wind at and height of the lowest model level, respectively, and c_d the surface drag coefficient mentioned above. Using $\sigma_{top} = 0.85$ and $\sigma_{strato} = 0.1$, the eddy diffusivity decays by about a factor of 10 at 700 hPa (Reed & Jablonowski, 2012). In ICON, $\sigma = \frac{p}{p_{surf}}$ and in CAM $\sigma = \frac{p}{10^5 Pa}$. While this can lead to different boundary layer depths over topography, the effect on zonal mean winds is negligible. The drag coefficient is constant over the ocean. Over land, an orographic factor c_{oro} that scales with the square root of the height of orography is added to that constant.

$$c_d = c_{ocean} + c_{oro} * \sqrt{h} \tag{3}$$

The rationale for this simple representation of subgrid orography is that the largest mountain ranges also tend to contain the steepest slopes and thus largest subgridscale variability. The form of the equation and

Table 1
Drag Settings for the Experiments

Experiment name	Model	Years	Topo	Season	Drag	Drag strength over Ocean	Drag strength over Land	Polar vortex
hs	ICON	51	yes	summer	Rayleigh	$\tau_F = 1$ day		no
ocr1	ICON	11	yes	summer	Rayleigh	$\tau_F = 1$ day	$\tau_F = 0.1$ days	no
ocr2	ICON	11	yes	summer	Rayleigh	$\tau_F = 1$ day	$\tau_F = 0.5$ day	no
hs_cam	CAM5	51	yes	summer	Rayleigh	$\tau_F = 1$ day		no
ocr1_cam	CAM5	11	yes	summer	Rayleigh	$\tau_F = 1$ day	$\tau_F = 0.1$ day	no
ocr2_cam	CAM5	11	yes	summer	Rayleigh	$\tau_F = 1$ day	$\tau_F = 0.5$ days	no
qd1	ICON	11	yes	summer	quadratic	Cd = 0.01	Cd = 0.025	no
qd2	ICON	11	yes	summer	quadratic	Cd = 0.01		no
qd3	ICON	11	yes	summer	quadratic	Cd = 0.01	Cd = 0.1	no
qd4	ICON	11	yes	summer	quadratic	Cd = 0.005	Cd = 0.01	no
qd5	ICON	11	yes	summer	quadratic	Cd = 0.001	Cd = 0.01	no
qd1n	ICON	11	no	summer	quadratic	Cd = 0.01	Cd = 0.025	no
qd2n	ICON	11	no	summer	quadratic	Cd = 0.01		no
qd3n	ICON	11	no	summer	quadratic	Cd = 0.01	Cd = 0.1	no
sdc3	ICON	26	yes	summer	quadratic	Cd = 0.01		no
sdc4	ICON	26	yes	summer	quadratic	Cd = 0.02		no
sdc6	ICON	26	yes	summer	quadratic, f(h)	Cd = 0.01	$Cd = 0.01+0.001\sqrt{h}$	no
sdc6y40	as sdc6, but meridional temp. gradient in Held-Suarez dTy = 40 K instead of 60.							
sdc6y80	as sdc6, but meridional temp. gradient in Held-Suarez dTy = 80 K instead of 60.							
sdc7	ICON	26	yes	summer	quadratic, f(h)	Cd = 0.01	$Cd = 0.01+0.0002\sqrt{h}$	no
sdc14	ICON	26	yes	summer	quadratic, f(h)	Cd = 0.02	$Cd = 0.02+0.001\sqrt{h}$	no
sdc9	ICON	26	yes	winter	quadratic	Cd = 0.01		no
sdc10	ICON	26	yes	winter	quadratic	Cd = 0.02		no
sdc11	ICON	26	yes	winter	quadratic, f(h)	Cd = 0.01	$Cd = 0.01+0.001\sqrt{h}$	no
sdc21	ICON	26	yes	winter	quadratic, f(h)	Cd = 0.01	$Cd = 0.01+0.0002\sqrt{h}$	no
sdc32	ICON	26	yes	winter	quadratic, f(h)	Cd = 0.01	$Cd = 0.01+0.0005\sqrt{h}$	no
sdc23	ICON	26	yes	winter	quadratic, f(h)	Cd = 0.01	$Cd = 0.01+0.001\sqrt{h}$	$\gamma = -4$
sdc24	ICON	26	yes	winter	quadratic	Cd = 0.01		$\gamma = -4$
sdc25	ICON	26	yes	winter	quadratic	Cd = 0.02		$\gamma = -4$
sdc26	ICON	26	yes	winter	quadratic, f(h)	Cd = 0.01	$Cd = 0.01 + 0.0005\sqrt{h}$	$\gamma = -4$
sdc27	ICON	26	yes	winter	quadratic, f(h)	Cd = 0.01	$Cd = 0.01 + 0.0002\sqrt{h}$	$\gamma = -4$
sdc28	ICON	26	yes	winter	quadratic, f(h)	Cd = 0.01	$Cd = 0.01 + 0.00035\sqrt{h}$	$\gamma = -4$
sdc9_cam	CAM5	26	yes	winter	quadratic	Cd = 0.01		no
sdc10_cam	CAM5	26	yes	winter	quadratic	Cd = 0.02		no
sdc11_cam	CAM5	26	yes	winter	quadratic, f(h)	Cd = 0.01	$Cd = 0.01+0.001\sqrt{h}$	no
sdc21_cam	CAM5	26	yes	winter	quadratic, f(h)	Cd = 0.01	$Cd = 0.01+0.0025\sqrt{h}$	no
sdc23_cam	CAM5	26	yes	winter	quadratic, f(h)	Cd = 0.01	$Cd = 0.01+0.0055\sqrt{h}$	no

Quadratic drag: simple drag scheme by Reed and Jablonowski (2012); f(h) = height-dependent drag over land (see text). γ = lapse rate in the stratosphere Polvani and Kushner (2002).

the range of values used for c_{oro} have been chosen to be consistent with reported drag coefficients over the continents (Garratt, 1977).

The simple drag setup is conceptionally similar to that used by Mbengue and Woollings (2019) but differs in the dependence of the drag coefficient on topography and the additional use of resolved topography in our setup.

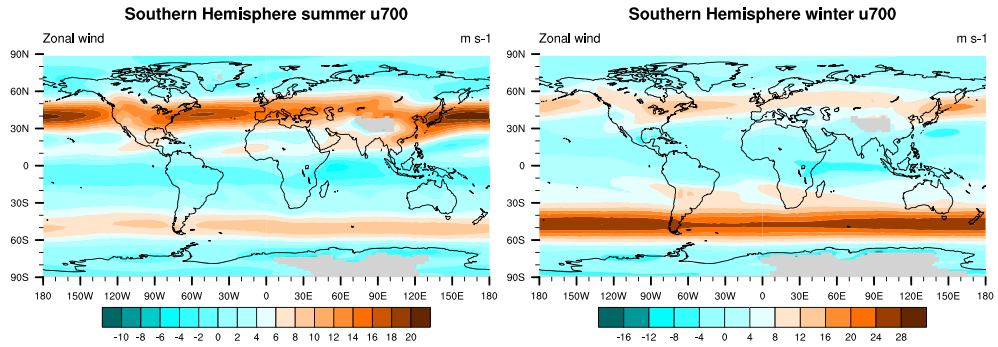

Figure 1. Zonal wind at 700 hPa in the Southern Hemisphere for (left) the summer setup using Rayleigh drag (hs) and (right) a winter setup using quadratic drag (sdc9) in the ICON model.

2.2. Experiments

Experiments and parameter settings are listed in Table 1. The first year of each run is discarded as spin-up. In the "qd" and "ocr" experiments, drag over land is independent of topography.

2.3. Data Analysis

To obtain the jet latitude, zonal mean zonal wind at 700 hPa is interpolated between the maximum and the two adjacent grid points on either side using cubic spline interpolation. Annular mode time scales are obtained by computing the EOF time series of the latitude-weighted zonal mean surface pressure. The annular mode time scale τ is obtained from the best exponential fit to the autocorrelation function over the first e-folding (Gerber et al., 2008).

3. Results

Combining Rayleigh or quadratic drag with realistic resolved topography results in a qualitatively realistic distribution of lower tropospheric westerlies with a circumglobal Southern Hemisphere midlatitude jet and distinct jet maxima over the Pacific and Atlantic ocean basins in the Northern Hemisphere (Figure 1).

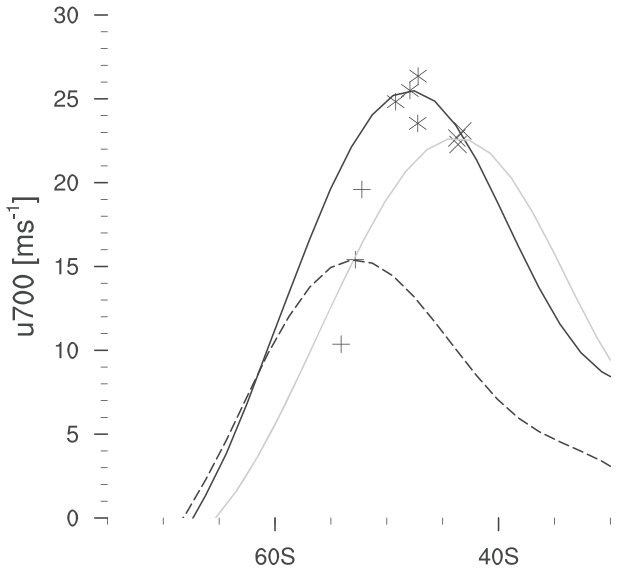

Figure 2. Zonal mean zonal wind (lines) and jet maxima (markers) for different configurations of ICON (black) and CAM5 (gray) with quadratic drag and topography. Dashed line and plus signs show summer seasonal settings; full lines and asterisks (ICON)/crosses (CAM) are for winter. Experiments used: sdc11,21,23_cam for CAM; sdc11,9,10,23 (winter) and 6,6y40 and 6y80 (summer) for ICON.

3.1. Jet Latitude as a Function of Dynamical Core, Forcing, and Surface Drag

Differences in jet characteristics between climate models can be caused by physical processes, namely, the temperature gradients generated by diabatic processes such as radiation or cloud formation (Ceppi et al., 2012), surface fluxes of heat and moisture (Polichtchouk & Shepherd, 2016), or drag that is represented in a model by resolved orography and parameterized drag processes (Pithan et al., 2016). Discretization choices for the dynamical core such as resolution and grid (horizontal and vertical), boundary conditions, the choice of vertical coordinate, the numerical schemes used to discretize the equations, or damping schemes to ensure numerical stability can also affect jet characteristics but should ideally be second order to the choice of physical parameters (Gerber et al., 2008; Polichtchouk & Cho, 2016).

Using the same Held-Suarez forcing in both ICON and CAM with topography and quadratic drag results in different zonal wind distributions and a difference in jet latitudes of about 5° (Figure 2, black line for ICON and gray line for CAM5). Changes to the drag parameter result in much smaller changes in jet latitude (Figure 2, asterisks for ICON and crosses for CAM5). Only changing the seasonal settings from Southern Hemisphere winter to summer (dashed black line, ICON) results in a jet shift of similar magnitude as the intermodel difference. This corresponds to a

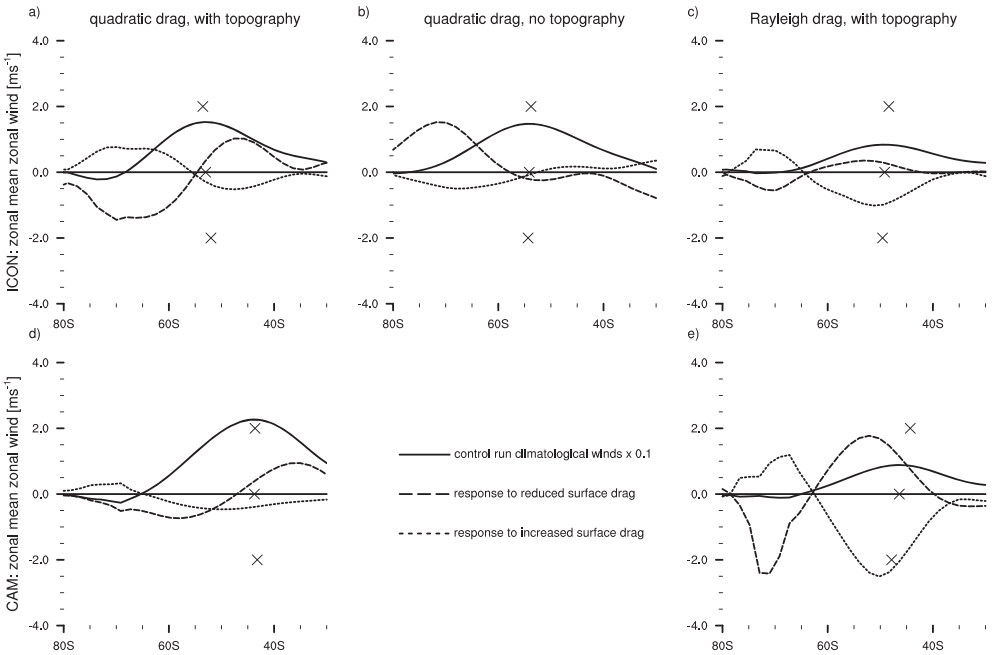

Figure 3. Effect of varying surface drag over land on zonal mean zonal winds for (a) and (d) quadratic drag and topography, (b) quadratic drag without topography, and (c) and (e) linear (Rayleigh) drag with topography. Crosses denote the jet latitude for each experiment, with stronger surface drag corresponding to a higher position on the *y* axis. Most runs use summer seasonal settings; only the CAM experiments in panel (d) are for winter. Results shown here correspond to the experiments qd1, qd2, and qd3 for panel (a); sdc11_cam, sdc21_cam, and sdc23_cam for CAM for panel (d); qd1n, qd2n, and qd3n for panel (b); hs, ocr1, and ocr2 for panel (c); and hs_cam, ocr1_cm, and ocr2_cam for panel (e).

7° shift in the region of maximum surface temperature gradient for the equilibrium temperature used for Newtonian relaxation. The intermodel difference is thus of the same magnitude as a substantial shift in the location of the maximum meridional gradient in the forcing. Note that in this setup, the intermodel difference can only be caused by the dynamical core and resolved topography, since all simplified physics are the same between our two models. It should be kept in mind that ICON solves a nonhydrostatic set of equations, whereas CAM solves hydrostatic primitive equations. However, nonhydrostatic effects are not important for horizontal scales greater than 10 km (e.g., Daley, 1988), which is way below resolved scales considered in this study or climate models. Therefore, the reasons behind the intermodel differences are likely due to the choice of resolution (vertical or horizontal), model top, vertical coordinate, or numerical methods used to discretize the governing equations.

Even substantial changes to the drag parameter over 1 order of magnitude within one model have much smaller effects than the difference between dynamical cores. Changing the strength of the meridional temperature gradient in one model and one season can substantially change the jet strength but has a small effect on the jet latitude (black plus signs in Figure 2). In this case, the stronger jets are located further equatorward, which is the opposite behavior to that found by Kidston and Vallis (2012).

3.2. Effect of Drag on Jet Latitude

As stated in section 1, results from dry Held-Suarez type models in which the jet shifts equatorward in response to increased surface drag are at odds with climate model sensitivity experiments where the Southern Hemisphere jet shifts poleward in response to increased surface drag (Chen et al., 2007; Mbengue & Woollings, 2019; Pithan et al., 2016; van Niekerk et al., 2017). As the concept of one circumglobal jet really only applies to the Southern Hemisphere and the role of zonal asymmetries is obvious for the Northern Hemisphere, zonally symmetric setups have mostly been used as an analog of the Southern Hemispheric circulation.

With quadratic drag and topography, increasing the drag over land leads to a poleward shift of the jet, whereas with linear (Rayleigh) drag and topography, increasing the drag over land leads to an equatorward

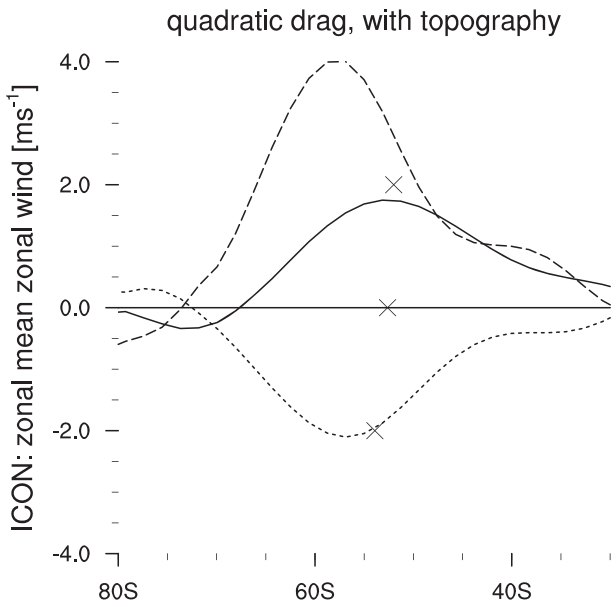

Figure 4. Effect of varying surface drag over ocean on zonal mean zonal winds for quadratic drag and topography; lines and symbols as in Figure 3. Results shown here correspond to the experiments qd2, qd4, and qd5.

shift of the jet. In the presence of topography, the zonal mean zonal wind response at 700 hPa to changes in the drag strength over land is qualitatively similar for the quadratic (Figure 3a) and linear (Figure 3c) drag schemes. Increased drag over land weakens the westerly winds on the equatorward side of the midlatitudes and leads to stronger winds on the poleward side, especially over the Southern Ocean. However, both the maximum response and the change from positive to negative response are located 5° to 10° further equatorward in the quadratic drag run, whereas the control run jet maximum is located somewhat further poleward for the quadratic than the linear drag setup. This results in a poleward shift of the jet with increased drag over land in the quadratic drag setup but an equatorward shift of the jet in the linear drag setup. In contrast, in the absence of topography (Figure 3b), increased quadratic drag over land leads to a small decrease of the zonal mean zonal wind on the poleward side and an increase on the equatorward side of the jet, resulting in an equatorward shift of the jet position. Note that while the CAM runs in Figure 3d are for a different season and drag settings than the ICON runs in Figure 3a, using more consistent settings in ICON does not qualitatively affect the results (not shown).

Increasing the drag strength over ocean in a setup with quadratic drag and topography leads to an equatorward jet shift (Figure 4). In this case, the wind speed changes in the same direction over most of the Southern Hemisphere, but the increase is stronger on the poleward side of the jet.

Our results are consistent with those of Mbengue and Woollings (2019) who use quadratic drag in a dry model without topography and report an equatorward shift of the Southern Hemisphere jet in response to increased drag over ocean and a similar but weaker response to increase drag over land. The equatorward shift of the jet in response to enhanced ocean drag in our experiments is also consistent with results from models using zonally symmetric boundary conditions and uniform, linear drag (Chen et al., 2007).

If only the change in the latitude of the jet maximum is taken into account, both the linear setup with topography and the quadratic drag case without topography show an equatorward shift for stronger drag values, similar to results for Rayleigh drag without topography (Chen et al., 2007). The poleward shift of the jet in response to stronger drag over land in the quadratic drag setup with topography conforms with sensitivity experiments using full-physics climate models that also show a poleward shift of the jet in response to increased orographic drag (Pithan et al., 2016; van Niekerk et al., 2017).

The opposite responses of the jet latitude to increases in drag over land and ocean (in the presence of topography and using quadratic drag) might be due to stationary wave dynamics or the latitudinal localization of drag. Increasing drag over ocean acts at all latitudes, whereas increasing the drag over land corresponds to a mechanical forcing on the equatorward flank of the jet, which has been shown to shift the jet poleward in idealized setups (Ring & Plumb, 2008). While the forcing is longitudinally confined to the small sections covered by land and topography (mostly the Andes, with a small contribution from Tasmania and New Zealand), the wind speed response is annular mode-like and almost zonally symmetric (not shown). This suggests that the flow in our model is dynamically annular at these latitudes (Gerber & Thompson, 2017). In the case of Rayleigh drag with topography, the initial jet position is somewhat further equatorward. As the location of the mechanical forcing is largely fixed by the position of continents and topography, this results in a forcing that is more centered on the jet and less accentuated on its equatorward flank.

The above results also emphasize that reporting changes in the jet latitude alone, as is frequently done in idealized studies on the midlatitude jet, is not enough to clearly characterize changes in the jet. Increasing the drag over land leads to an equatorward shift of the jet both for quadratic drag without topography (Figure 3b) and linear drag with topography (Figure 3c), but the underlying changes in zonal mean zonal winds differ substantially.

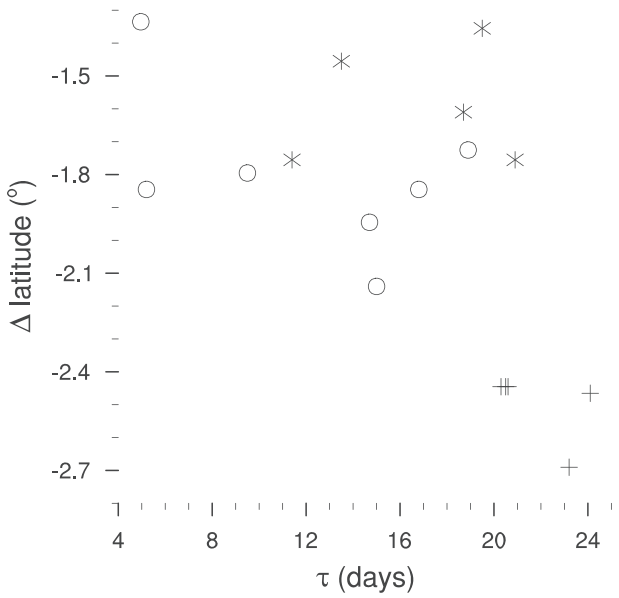

Figure 5. Annular mode time scale versus poleward shift in response to tropical heating for summer (stars), winter without vortex (plus signs), and winter with stratospheric vortex (circles) setups for ICON. Experiments used: tc_sdc3,4,6,7,14 (summer), tc_sdc9,10,11,21,32 (winter w/o vortex), and tc_sdc23-28 (winter with vortex).

3.3. Relationship Between Annular Mode Time Scale and Jet Shift

In the dry model with topography and quadratic surface drag, no universal relationship between annular mode time scale and jet shift in response to tropical tropospheric warming is apparent, neither in Southern Hemisphere summer nor in winter, with or without stratospheric polar vortex (Figure 5 for ICON). The figure may generate an overall impression of a trend toward stronger jet shifts at longer time scales; however, this is solely due to the wintertime experiments without stratospheric vortex, which display longer time scales and stronger jet shifts than other experiments. This lack of support for the fluctuation-dissipation theorem as an explanation for intermodel differences is consistent with a seasonal analysis of CMIP5 models (Simpson & Polvani, 2016) and questions the applicability of the fluctuation-dissipation theorem to the jet latitude variability and climate change response.

4. Conclusions

Intermodel differences in jet latitude between ICON and CAM5 in a Held-Suarez-like experiment with topography and quadratic drag are substantially greater than changes in jet latitude obtained by changing the drag parameter over land by 1 order of magnitude. Large changes in the shape of the Newtonian relaxation profile are required to obtain a jet shift of similar magnitude as the intermodel difference. This suggests that aspects related to models' resolved processes such as the representation of resolved topography, vertical and horizontal resolution, the numerical schemes used in the dynamical core, and damping schemes to ensure numerical stability can play an important role in generating intermodel spread and model biases in the extratropical jet in CMIP intercomparisons.

Using real-world topography and a surface drag that quadratically depends on wind speed in a dry dynamical core changes the sign of the jet response to increased drag over land compared to the standard Held-Suarez setup with linear drag and no topography. In a standard Held-Suarez setup, increased Rayleigh drag at the surface leads to an equatorward shift of the jet (Chen et al., 2007). A model with quadratic drag and no topography also responds with an equatorward jet shift when drag is increased over real-world land areas only (Mbengue & Woollings, 2019). In our setup with topography and quadratic drag, increased drag over land leads to a poleward shift of the jet, as does increased orographic drag in complex climate models (Pithan et al., 2016; van Niekerk et al., 2017).

While Held-Suarez models have been reported to display a fluctuation-dissipation relationship between jet latitude variability in a control run and the jet latitude shift in response to forcing, no such relationship is

found in our model with topography and quadratic drag. The absence of such a link is consistent with a recent analysis of CMIP5 models (Simpson & Polvani, 2016).

Our results support the idea that the gap in complexity between idealized models and dynamical theory on the one side and complex climate models on the other side has become too wide (Held, 2005) to use the established simple models to understand complex model results such as the jet sensitivity to surface drag. Our work suggests that a dry dynamical core with real-world topography and a drag scheme that is more physical than Rayleigh drag is a useful addition to the model hierarchy. This setup remains limited to dry dynamics and yet manages to reproduce several aspects of the behavior of complex models that a standard Held-Suarez approach fails to capture. Intercomparing results from a greater number of climate models in dry dynamics setups with and without topography would provide a basis to understand if and how discretization choices for the resolved dynamics affect important climate characteristics such as the jet latitude.

Acknowledgments
Thanks to two anonymous reviewers whose comments and suggestions have helped us to improve the present manuscript. F. P. acknowledges support from the Helmholtz Society through the Helmholtz Postdoc project "Understanding the role of atmosphere-surface coupling for large-scale dynamics." Model results have been archived in the DKRZ long-term achive LTA-doku and can be retrieved online (at http://cera-www.dkrz.de/WDCC/ui/Compact.jsp?acronym=DKRZ_LTA_995_ds00002). Model codes are available via the Max Planck institute for Meteorology (subject to a license agreement) for ICON and the National Center for Atmospheric Research for CAM.

References

Bony, S., Stevens, B., Frierson, D. M., Jakob, C., Kageyama, M., Pincus, R., et al. (2015). Clouds, circulation and climate sensitivity. *Nature Geoscience*, *8*(4), 261–268.

Brayshaw, D. J., Hoskins, B., & Blackburn, M. (2009). The basic ingredients of the North Atlantic storm track. Part I: Land–sea contrast and orography. *Journal of the Atmospheric Sciences*, *66*(9), 2539–2558.

Ceppi, P., Hwang, Y.-T., Frierson, D. M., & Hartmann, D. L. (2012). Southern Hemisphere jet latitude biases in CMIP5 models linked to shortwave cloud forcing. *Geophysical Research Letters*, *39*, L19708. https://doi.org/10.1029/2012GL053115

Chang, E. K. (2009). Diabatic and orographic forcing of northern winter stationary waves and storm tracks. *Journal of Climate*, *22*(3), 670–688.

Chen, G., Held, I. M., & Robinson, W. A. (2007). Sensitivity of the latitude of the surface westerlies to surface friction. *Journal of the Atmospheric Sciences*, *64*(8), 2899–2915.

Cohen, J., Screen, J. A., Furtado, J. C., Barlow, M., Whittleston, D., Coumou, D., et al. (2014). Recent Arctic amplification and extreme mid-latitude weather. *Nature geoscience*, *7*(9), 627.

Daley, R. (1988). The normal modes of the spherical non-hydrostatic equations with applications to the filtering of acoustic modes. *Tellus A*, *40*(2), 96–106.

Garratt, J. (1977). Review of drag coefficients over oceans and continents. *Monthly weather review*, *105*(7), 915–929.

Gerber, E. P., Polvani, L. M., & Ancukiewicz, D. (2008). Annular mode time scales in the Intergovernmental Panel on Climate Change fourth assessment report models. *Geophysical Research Letters*, *35*, L22707. https://doi.org/10.1029/2008GL035712

Gerber, E. P., & Thompson, D. W. (2017). What makes an annular mode "annular"? *Journal of the Atmospheric Sciences*, *74*(2), 317–332.

Gerber, E. P., Voronin, S., & Polvani, L. M. (2008). Testing the annular mode autocorrelation time scale in simple atmospheric general circulation models. *Monthly Weather Review*, *136*(4), 1523–1536.

Giorgetta, M. A., Brokopf, R., Crueger, T., Esch, M., Fiedler, S., Helmert, J., et al. (2018). ICON-A, the atmosphere component of the ICON Earth System Model. Part I: Model description. *Journal of Advances in Modeling Earth Systems*, *10*, 1613–1637. https://doi.org/10.1029/2017MS001242

Held, I. M. (2005). The gap between simulation and understanding in climate modeling. *Bulletin of the American Meteorological Society*, *86*(11), 1609–1614.

Held, I. M., & Suarez, M. J. (1994). A proposal for the intercomparison of the dynamical cores of atmospheric general circulation models. *Bulletin of the American Meteorological Society*, *75*(10), 1825–1830.

James, I., & Gray, L. (1986). Concerning the effect of surface drag on the circulation of a baroclinic planetary atmosphere. *Quarterly Journal of the Royal Meteorological Society*, *112*(474), 1231–1250.

Kidston, J., & Gerber, E. (2010). Intermodel variability of the poleward shift of the austral jet stream in the CMIP3 integrations linked to biases in 20th century climatology. *Geophysical Research Letters*, *37*, L09708. https://doi.org/10.1029/2010GL042873

Kidston, J., & Vallis, G. (2012). The relationship between the speed and the latitude of an eddy-driven jet in a stirred barotropic model. *Journal of the Atmospheric Sciences*, *69*(11), 3251–3263.

Mbengue, C. O., & Woollings, T. (2019). The eddy-driven jet and storm-track responses to boundary-layer drag: Insights from an idealized dry GCM study. *Journal of the Atmospheric Sciences*, *76*, 1055–1076.

McGraw, M. C., & Barnes, E. A. (2016). Seasonal sensitivity of the eddy-driven jet to tropospheric heating in an idealized AGCM. *Journal of Climate*, *29*(14), 5223–5240.

Neale, R. B., Gettelman, A., Park, S., Conley, A. J., Kinnison, D., Marsh, D., et al. (2010). Description of the NCAR Community Atmosphere Model (CAM 5.0) (*Tech. Note NCAR/TN-486+STR,*): NCAR.

Pithan, F., Shepherd, T. G., Zappa, G., & Sandu, I. (2016). Climate model biases in jet streams, blocking and storm tracks resulting from missing orographic drag. *Geophysical Research Letters*, *43*, 7231–7240. https://doi.org/10.1002/2016GL069551

Polichtchouk, I., & Cho, J.-K. (2016). Equatorial superrotation in Held and Suarez like flows with weak equator-to-pole surface temperature gradient. *Quarterly Journal of the Royal Meteorological Society*, *142*(696), 1528–1540.

Polichtchouk, I., & Shepherd, T. (2016). Zonal-mean circulation response to reduced air–sea momentum roughness. *Quarterly Journal of the Royal Meteorological Society*, *142*(700), 2611–2622.

Polvani, L. M., & Kushner, P. J. (2002). Tropospheric response to stratospheric perturbations in a relatively simple general circulation model. *Geophysical Research Letters*, *29*(7), 18–1. https://doi.org/10.1029/2001GL014284

Reed, K. A., & Jablonowski, C. (2012). Idealized tropical cyclone simulations of intermediate complexity: A test case for AGCMs. *Journal of Advances in Modeling Earth Systems*, *4*, M04001. https://doi.org/10.1029/2011MS000099

Ring, M. J., & Plumb, R. A. (2008). The response of a simplified GCM to axisymmetric forcings: Applicability of the fluctuation–dissipation theorem. *Journal of the Atmospheric Sciences*, *65*(12), 3880–3898.

Robinson, W. A. (1997). Dissipation dependence of the jet latitude. *Journal of climate*, *10*(2), 176–182.

Shepherd, T. G. (2014). Atmospheric circulation as a source of uncertainty in climate change projections. *Nature Geoscience*, *7*(10), 703–708.

Simpson, I. R., & Polvani, L. M. (2016). Revisiting the relationship between jet position, forced response and annular mode variability in the southern mid-latitudes. *Geophysical Research Letters*, *43*, 2896–2903. https://doi.org/10.1002/2016GL067989

van Niekerk, A., Scinocca, J. F., & Shepherd, T. G. (2017). The modulation of stationary waves, and their response to climate change, by parameterized orographic drag. *Journal of the Atmospheric Sciences*, *74*(8), 2557–2574.

Wilson, C., Sinha, B., & Williams, R. G. (2009). The effect of ocean dynamics and orography on atmospheric storm tracks. *Journal of Climate*, *22*(13), 3689–3702.